# Influence of third-harmonic fields on multiphoton ionization of noble gases in unfocused laser beams

W. R. Garrett, W. R. Ferrell, M. G. Payne, and John C. Miller
*Chemical Physics Section, Oak Ridge National Laboratory, Oak Ridge, Tennessee 37831*
(Received 16 January 1986)

Unfocused linearly polarized laser beams, in single-pass and counterpropagating configurations, are used in conjunction with absolute ionization measurements in calibrated proportional counters to examine the nature of multiphoton ionization of xenon near three-photon resonances. Mixtures of xenon with other noble gases are also used to incorporate phase matching in order to elucidate additional characteristics of multiphoton ionization in the presence of third-harmonic fields. Point-by-point comparisons are made between theoretically predicted and experimentally observed features of the study. We also show how detailed information on multiphoton ionization involving phase-matched third-harmonic photons can be used to obtain optical constants in the vacuum-ultraviolet region.

## I. INTRODUCTION

In a detailed theoretical study concurrent with the present paper, Payne, Garrett, and Ferrell[1] have discussed recent experimental[2–7] and theoretical work[8–13] on multiphoton-ionization studies in noble gases in spectral regions near three-photon resonances that can also be excited by a one-photon transition. In this theoretical study (hereafter referred to as I) quantitative analytical descriptions are given of the on-resonance cancellation effect that develops between three-photon excitation and excitation by the coherently generated third-harmonic field and of the partial spoiling of this effect in the presence of counterpropagating beams. The latter effect causes three-photon resonant enhancement of multiphoton ionization (MPI) to reappear at elevated pressures where, in the subset of interest, it is totally unobservable with a single laser beam. The authors also quantitatively describe third-harmonic generation with unfocused beams on the negatively dispersive side of three-photon resonances in the presence of a phase-matching buffer gas. The strong influence of dimer absorption on third-harmonic production in the phase-matching gas mixture is described and new features are predicted for the third-harmonic profiles or "lineshapes" for generation by unfocused beams. Details of the pressure-dependent behavior of MPI involving phase-matched third-harmonic photons is also analytically described. Finally, in the theoretical study it is shown how the quantitative description of third-harmonic generation, and the resultant MPI signals, can be used to determine oscillator strengths of resonances with which third-harmonic generation is associated, the coefficients for absorption by active-gas–buffer-gas dimers, and the difference of the indices of refraction of the buffer gas at the fundamental and third-harmonic frequencies.

In I a concerted effort was made to treat the MPI problem in a comprehensive but tractable manner with reference to excellent agreement between the theory and earlier experimental results, including a detailed study by Payne *et al.*[8] Due to the requisite length of the theoretical discourse, no new comparisons with experiment were made in the paper.

In order to demonstrate the adequacy of our description of MPI processes involving third-harmonic fields, we will, in Secs. II A–III D, make a point-by-point comparison between some of those predictions and corresponding results from a set of experiments conducted specifically for this purpose. We then show how detailed information from MPI measurements with visible photons can be used to determine atomic parameters in the vacuum-ultraviolet (vuv) spectral region. Finally, in Sec. II E, we will show how third-harmonic production can very strongly influence MPI of certain two-photon allowed transitions through a two-photon process involving absorption of a third-harmonic photon and a laser photon, and we will give a theoretical discussion of the effect.

## II. EXPERIMENTAL METHOD

In the present study we have investigated several aspects of MPI processes in xenon and mixtures of xenon with buffer gases (argon or krypton), using unfocused laser beams in single-pass and counterpropagating geometries. Though resultant ionization signals in noble gases are small, the use of unfocused beams allows the detailed theoretical analysis[1] of MPI to be tested experimentally.

In order to make ionization measurements over wide ranges of pressure, with various buffer-gas concentrations for phase matching, high-sensitivity gas proportional counters of special design were used as ionization detectors. Considerable difficulty is encountered in obtaining quantitative data on MPI studies where ionization signals can be quite small (for power densities less than $10^8$ W/cm$^2$), such that gas amplification is required for signal detection. A change in gas pressure is accompanied by a change in the gain of the gaseous amplification feature of the ionization detector. This feature has been present in earlier experimental studies.[2,4,6,7,14] Thus, in order to make quantitative MPI measurements, independent cali-

 

bration of ionization signals is required at every pressure; otherwise, major uncertainties arise in ionization yields even in measurements of relative signals at different pressures.

In this study absolute ionization signals were measured using calibrated gas proportional counters, one of which is depicted in Fig. 1. The proportional counters provided electron detection of high sensitivity ($<10$ electrons) and low noise to produce signals which were proportional to the number of electrons that resulted from ionization in the laser beam.[15] Field tubes (guard electrodes) eliminated the detection of electrons generated within 3.8 cm of either window of the ionization cell and made possible the elimination of any overlap between the incident laser beam and reflections from the back cell window. Absolute determination of the ionization signals was made by comparison with known ionization yields from internal absorption of 5900-eV x rays from an $^{55}$Fe source. Photoelectrons from this source generate $\sim 270$ ionizations in Xe, Kr, Ar, Ne, or mixtures of these gases when number densities and path lengths are sufficiently high to stop the photoelectrons inside the counter volume. There are no geometrical corrections to the calibration because all gain within the gas occurs in a small region very near the wire which forms the positive electrode of the counter. Ionization yields could be determined over a wide range extending from less than ten to several hundred thousand electrons.

In one set of experiments, described below, a Lambda Physik excimer- (EMG 101) pumped dye laser (FL-2000E) of (1—15)-mJ output in ($\sim$10—12)-ns pulses of $\sim 1.5$-cm$^{-1}$ bandwidth was used in a configuration shown schematically in Fig. 2. Signals were detected by a charge-sensitive preamplifier and simultaneously displayed on an oscilloscope and processed by a Princeton Applied Research boxcar integrator. The time-averaged signals were then recorded on an $x$-$y$ plotter.

In a second set of experiments a Lumonics (861T) excimer-pumped dye-laser system (EDP 330) was used. Total energy per pulse was lower (1—8 mJ), pulse length was shorter ($\sim$4 ns), and bandwidth was narrower (0.3 cm$^{-1}$) than the arrangement described above.

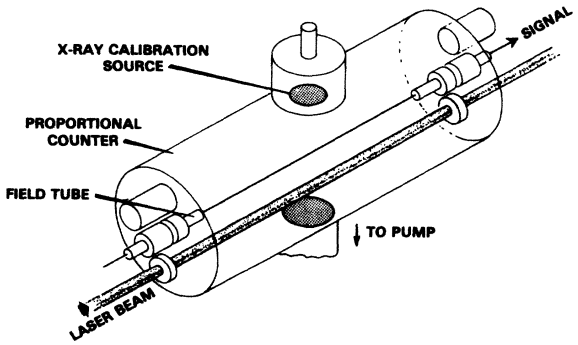


FIG. 1. Proportional counter showing field tubes or guard rings, removable x-ray calibration source, and laser-beam path. Length of proportional counter region between field tubes is 11.5 cm.

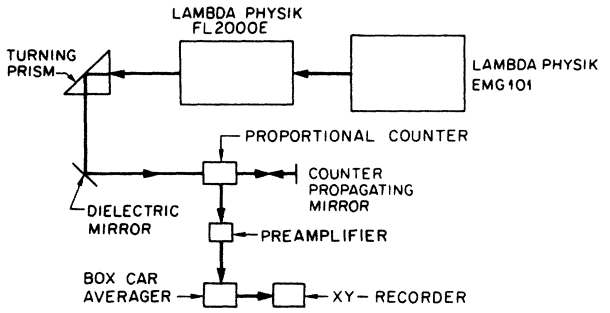


FIG. 2. First experimental setup: Lambda Physik excimer laser and dye laser, proportional counter, quartz optics, and electronics.

## III. EXPERIMENTAL RESULTS

### A. Multiphoton ionization of xenon at exact three-photon resonances

On the basis of theoretical estimates of relevant three-photon Rabi frequencies $\Omega_3(t)$, we conclude that with our present complement of lasers and ionization detectors, and if the third-harmonic cancellation effect was *not* operative, we should be able to observe three-photon resonantly enhanced MPI in xenon via several accessible states (i.e., $6s[\frac{3}{2}]\ J=1$, $6s'[\frac{1}{2}]\ J=1$, $5d[\frac{3}{2}]\ J=1$, and $7s[\frac{3}{2}]\ J=1$) even with *unfocused* beams. Also, in the absence of the cancellation effect the ionization signals should be shifted from the resonance position only by the ac Stark shift, they should be proportional to the number density of the active gas, $N_A$, and they should be fourth or fifth order in laser intensity depending on the number of photons required to reach the continuum (fifth order at $6s$, fourth order at other higher levels). Moreover, according to the theoretical predictions of the preceding paper, this behavior should persist under broadband or narrow-band laser excitation and should be independent of collisional effects (unaffected by a buffer gas of number density $N_B$, even at very large $N_B$).

In the curves on the left of Fig. 3, we show ionization signals (number of electrons liberated within the 11.5-cm-long counting volume of the proportional counter of Fig. 1) in the region of the three-photon $6s$ resonance in pure xenon. With a single unfocused beam no resonant signal was observable with maximum laser power ($\sim 2\times 10^8$ W/cm$^2$), maximum proportional counter gain, and over a range of xenon pressures from $10^{-3}$ to 20 Torr. (Typical signal is marked "single beam" in Fig. 3.) The cooperative cancellation effect is sufficiently effective that no ionization ($<3$ ions/laser shot) was produced where thousands of electrons would have been expected on the basis of a simple extrapolation from earlier beam data.[3] However, with counterpropagating beams, very strong signals, of hundreds to many thousands of electrons, were easily observed at frequencies corresponding to any of the xenon resonances mentioned above over a wide range of

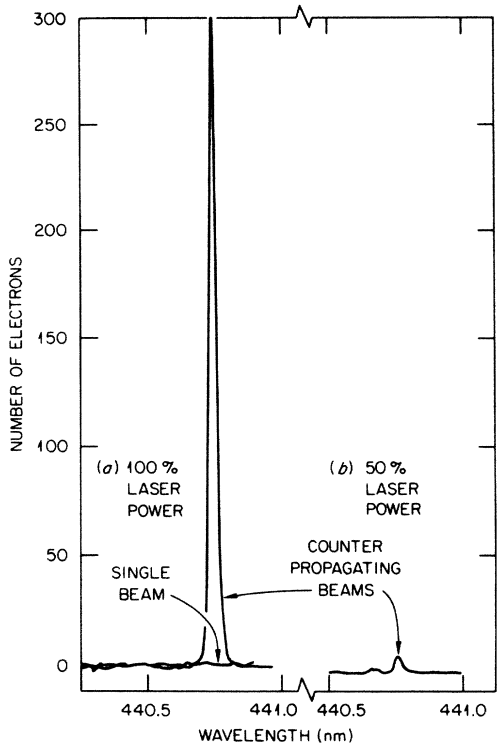


FIG. 3. (a) Comparison of the resonance signal for counterpropagating beams and the single-pass straight-through beam. (b) With counterpropagating geometry the resonance signal decreased by a factor of 32 as laser power was reduced by a factor of 2. Xenon pressure, $P_{Xe}=20$ Torr.

laser power, reflected-beam intensity, and target-gas pressure. Indeed, the enhancement at a given three-photon resonance is so effectively restored by a counterpropagating beam, that 8% reflections from a window or a microscope slide yield very appreciable resonant ionization signals at any of the three-photon levels examined. Typical data are shown in Fig. 3 as curve (a). (To eliminate spurious counterpropagating beams in the unidirectional beam experiments, care was taken to rotate the chamber in a manner such that window reflections did not overlap the incident beam.) We note that the theory indicates that the cancellation effect in our xenon examples is so complete that three-photon excitation of all the lowest optically allowed transitions becomes nullified at target-gas pressures as low as $10^{-4}$ Torr for a laser beam of 0.3 $cm^{-1}$ bandwidth or less, *and* that it persists up to many Torr even in the presence of rapid collisions from hundreds of Torr of a buffer gas. Experimentally, we found behavior similar to that of Fig. 3; that is, no signal in single-pass and large signals in counterpropagating geometry, in experiments with gas pressures from as low as $10^{-3}$ Torr to more than 100 Torr in xenon at the $6s[\frac{3}{2}]$ $J=1$, $6s'[\frac{1}{2}]$ $J=1$, $5d[\frac{3}{2}]$ $J=1$, and $7s[\frac{3}{3}]$ $J=1$ resonances, and in krypton at the $5s'[\frac{1}{2}]$ $J=1$ resonance. Identical results were obtained with argon and krypton buffer gases of one to several hundred Torr. Results were the same when laser bandwidths were changed over a factor of 5. All observed features were consistent with the analysis of Ref. 1.

In the counterpropagating geometry, all observed resonant excitations are due to the absorption of two photons from one beam and the third photon from the oppositely propagating second beam.[1,6,7,11] The one-photon Rabi pumping through the third-harmonic field is cancelled only by the component of the three-photon Rabi rate due to absorption of all three photons from a single beam. The six remaining terms of the total three-photon Rabi frequency which are due to absorption from two separate beams have no corresponding one-photon terms. Thus, the cooperative effect is not operative in the "mixed-beam" contribution to resonant excitation and the resulting signal should be $n$th order in the laser intensity (e.g., fifth order for ionization through the $6s$ state) and directly proportional to the xenon number density $N_A$ up to concentrations where pressure-broadened linewidths become larger than the laser bandwidth. In Fig. 3, curve (b), the counterpropagating signal is confirmed as being a fifth-order process for ionization through the $6s$ level of xenon. Note that a reduction by a factor of 2 in laser power results in a reduction factor of $\sim 32$ for the ionization signal. The calibrated signals are found to be proportional to the number density $N_A$ of the active or target gas when the laser bandwidth is larger than the pressure-broadened linewidth, and are independent of buffer-gas number density $N_B$.

### B. Functional dependence of cancellation spoiling in counterpropagating beams

We have shown in the previous theory[1] that when a fraction $f$ of an unfocused Gaussian laser beam of diameter $d$ and bandwidth $\sigma$ is reflected back on itself near the three-photon resonance frequency $\omega_r$, over a path length $L$, the rate of production of excited-state population by the "mixed-beam" three-photon absorption is

$$R_\omega = 3\pi^2 N_A d^2 (f+f^2) L \frac{|\Omega_3(t)|^2}{\sigma} \times \exp[-(3\omega-\omega_r)^2/6\sigma^2] . \quad (1)$$

This equation was derived assuming perfect spatial and temporal overlap of the counterpropagating beams. The three-photon Rabi frequency $\Omega_3(t)$ is defined in I.

In order to test the predicted functional form of the "spoiling" of the cancellation effect in partially reflected beams, we utilized a second experimental setup as shown in Fig. 4. In this instance the Lumonics excimer dye-laser system was used with a dual-chamber internally calibrated proportional counter system. For these experiments an LSI-11/03 computer-based data-acquisition system was used such that shot-by-shot readings of laser intensity, reflected intensity, and ionization signal could be simultaneously recorded and stored on floppy-disk storage for subsequent analysis. In order to control the reflected-beam intensity, two cube-type polarizing beam splitters (one of which was rotatable) were installed between the second ionization cell and the reflecting mirror (not shown in the figure). The fraction $f$ of the reflected-beam intensity

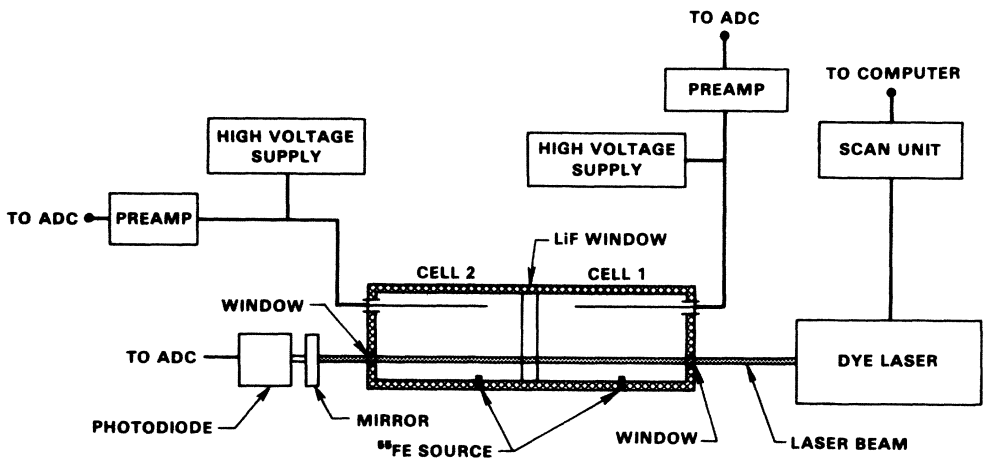


FIG. 4. Second experimental setup: Lumonics excimer laser and dye laser. Two proportional counters are independently operated and independently calibrated at individual pressures. Shot-by-shot data from proportional counters and from a laser-beam—intensity photodiode monitor are recorded on a LSI-11/03 computer system.

could be varied by rotating one of the polarizing beam splitters with respect to the other. Beam intensities were measured with calibrated photodiodes.

In Fig. 5 we show the ionization signal as a function of the reflected fraction $f$ of the on-resonance laser beam. The data are compared with the theoretical form from Eq. (1) where the ionization signal $S$ is given by the following: $S=\alpha(f+f^2)$. [The absolute value of $\Omega_3(t)$ is not measured.] We see that the cancellation "spoiling" behaves as predicted when a reflected beam of variable intensity is introduced. As expected, similar results were obtained with a buffer gas and, in experiments at other pressures of the active gas, ionization signals were proportional to $N_A$ and the functional form was independent of $N_A$ or $N_B$.

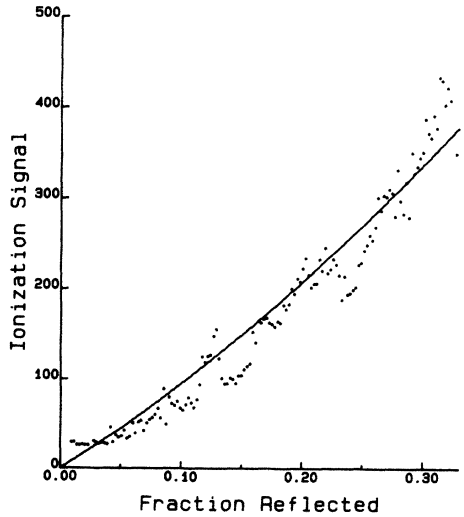


FIG. 5. Functional relationship between ionization at exact resonance (Xe 6$s$ level) and fraction of beam reflected in counterpropagating geometry. Pressure and input laser intensity held constant ($P_{Xe}=1$ Torr).

### C. Third-harmonic production and MPI profiles on the wing of a resonance line under phase-matching conditions

In the studies described above, resonantly enhanced MPI results at several exact three-photon $\Delta J=1$ resonances in xenon (and one in krypton) showed predicted behavior in single-pass and counterpropagating geometries. Observed results were unaffected by addition of a large quantity of a buffer gas (more than 100 Torr), i.e., no enhanced ionization occurred in single beams and strong three-photon resonance signals in counterpropagating geometry remained unchanged until the atomic linewidth due to pressure broadening exceeded the laser bandwidth. However, in contrast to this behavior, we know from theory that on the negatively dispersive side of three-photon resonances the generation of real third-harmonic photons can strongly influence MPI. Moreover, the presence of a positively dispersive buffer gas can greatly influence third-harmonic generation, and thus MPI, in frequency regions where phase matching can be attained. The dominant influence of third-harmonic generation and absorption on the MPI processes at phase matching can be made quite clear through a rather simple analysis.

In the regions of interest, near three-photon resonances, the perturbation-theory expression for the probability of MPI factors into a product of two terms, the first of which represents excitation into the resonant state at a detuning $\Delta_r$ from resonance, and a second factor which represents ionization out of the excited state. Thus, if we consider a crude square pulse model for the laser (pulse length $\tau$), then the probability of $n$-photon MPI of an atom by laser photons in a beam of flux $\Phi$ is

$$p_i \simeq \left| \frac{\Omega_3}{\Delta_r} \right|^2 \sigma_{n-3}(\omega)\Phi\tau \,, \tag{2}$$

where $\Omega_3$ is the three-photon Rabi frequency of the three-photon resonance and $\sigma_{n-3}(\omega)$ is the MPI cross sec-

tion for ionizing the nearby resonance level at frequency $\omega$ by $n-3$ photons. The cross section $\sigma_{n-3}(\omega) \propto I^{n-3}$ in the overall $n$-photon MPI process.

At the phase-matching frequency third-harmonic photons are produced at $3\omega$. The MPI probability resulting from absorption of one of these photons (rather than three laser photons) to reach the excited state with subsequent absorption of laser photons to reach the continuum can also be factored into two terms. The probability of ionizing an atom through third-harmonic absorption is

$$P_i' \simeq \left| \frac{\Omega_1}{\Delta_r} \right|^2 \sigma_{n-3}(\omega) \Phi \tau \,, \tag{3}$$

where $\Omega_1$ is the one-photon Rabi frequency associated with the third-harmonic field $E_{3\omega}$. The factor $\sigma_{n-3}(\omega)$ is the same as in Eq. (2). We also know that $\Omega_1$ is related to the third-harmonic field and the matrix element $D_{0,1}$ connecting the ground state and the excited state under discussion.[1] That is,

$$|\Omega_1|^2 = \left| \frac{E_{3\omega} D_{0,1}}{2\hbar} \right|^2 . \tag{4}$$

Neglecting absorption, a phase-matched unfocused beam produces a flux $\Phi_{3\omega}$ of third-harmonic photons on axis at depth $z$ into the medium,

$$\begin{aligned} \Phi_{3\omega}(z,t) &= (3!) 2\pi N_A^2 |D_{0,1}|^2 z^2 |\Omega_3(t)|^3 3\omega/\hbar c \Delta_r^2 \\ &= c E_{3\omega}^2 / 8\pi\hbar(3\omega) \,. \end{aligned} \tag{5}$$

Thus, we find

$$|\Omega_1|^2 \simeq \left( \frac{\kappa z}{\Delta_r} \right)^2 |\Omega_3|^2 \,, \tag{6}$$

where we have defined[1,10,11] $\kappa = 2\pi N_A |D_{0,1}|^2 \omega_r/\hbar c$. We see that the probability $P_i$ for MPI through three-photon excitation and subsequent ionization and that which proceeds by third-harmonic absorption, $P_i'$, are both proportional to $|\Omega_3|^2$. Thus, at a depth $z$ into the medium we can conveniently write the ratio of the two ionization probabilities in the simple form

$$\frac{P_I'}{P_I} = \left( \frac{\kappa z}{\Delta_r} \right)^2 . \tag{7}$$

In the experiments conducted in the present study this ratio becomes very large. For example, consider MPI in xenon at a frequency on the high-energy side of the $6s$ resonance. Then $\kappa = 2.4\times 10^{14} (\text{rad/s cm}) P_{\text{Xe}}(\text{Torr})$ for this level. If phase matching is produced at a detuning $\Delta_r = 200\ \text{cm}^{-1} \simeq 4\times 10^{13}$ rad/s from the resonance then at 1 cm into the gas cell

$$\frac{P_I'}{P_I} = \left( \frac{2.4\times 10^{15} P_{\text{Xe}}}{4\times 10^{13}} \right)^2 = 3600 P_{\text{Xe}}^2 . \tag{8}$$

With $P_{\text{Xe}} = 2$ Torr we have $P_I'/P_I = 1.4\times 10^4$. Thus, at the phase-matching frequency, in this example, the probability of producing ionization by the production and subsequent absorption of a third-harmonic photon is $\sim 10^4$ times more probable than MPI through the laser photons directly. Thus, under circumstances where phase-matched third-harmonic production take place, MPI spectra simply mimic third-harmonic production.[1]

On the basis of previous work by Castex,[16] we make one additional observation concerning phase-matched MPI on the blue wing of three-photon resonances in noble gases. The investigation by Castex[16] of dimer absorption of vuv light in noble-gas mixtures infers that in the phase-matching region of these systems dimer absorption should dominate the multiphoton process.[8] The mechanism is one in which weakly bound mixed dimers, though low in concentration, are initially excited with large cross section and subsequently dissociate into atoms in the nearby resonant state. The resonance population can thus be ionized by the absorption of the requisite number of laser photons at any time during the remainder of the laser pulse. (The latter is true, since due to radiation trapping the effective lifetime of the excited state is greater than the laser pulse length.) If we define the absorption coefficient for vuv photons as $2\beta$, then at room temperature experimental absorption coefficients under circumstances of interest here are of the form $2\beta = K(\omega,T) P_A P_B$, with the coefficient $K(\omega,T)$ being greater than $10^{-4}\ \text{Torr}^{-2}\,\text{cm}^{-1}$ near strong resonances in xenon-krypton and xenon-argon mixtures. Castex[16] has shown that under present circumstances, when dimer absorption occurs on the high-energy side of a resonance, the upper potential well of the $AB$ complex is either repulsive or very shallow so that, upon absorption, $(AB)^* \rightarrow A^* + B$. Thus, on the wing of a line each excitation leads to an excited atom in the nearby resonance state. At pressures of interest here the photons emitted by resulting excited atoms have mean free paths at line center of $10^{-3}$ cm or less. As just mentioned, strong radiation trapping of resonance photons occur and a long effective lifetime is produced for the resonance level. This picture of dimer absorption in the near-resonant ionization mechanism has also been confirmed in recent studies using two focused, independently tunable dye lasers.[17]

Having made these observations concerning details of the processes involved in MPI under phase-matched third-harmonic generation in noble-gas mixtures, we now wish to make a quantitative assessment of this process in relation to relevant theoretical predictions.[1] In this context it is useful to recount the conditions for phase matching between the laser and third-harmonic fields under conditions where an active gas, of number density $N_A$, is buffered by higher concentration of a buffer gas of number density $N_B$. The wave-vector mismatch $\Delta k$ between the laser field, of wave vector $k_\omega$, and the third-harmonic field, of wave vector $k_{3\omega}$, is

$$\begin{aligned} \Delta k = 3k_\omega - k_{3\omega} &= \frac{3\omega}{c}[n(\omega) - n(3\omega)] \\ &\simeq \frac{6\pi\omega}{c}[N_A \chi_A(\omega) + N_B \chi_B(\omega) \\ &\quad - N_A \chi_A(3\omega) - N_B \chi_B(3\omega)] \,, \end{aligned} \tag{9}$$

where the $n$'s are indices of refraction and the $\chi_A$ and $\chi_B$ are linear susceptibilities of the target and buffer gas, respectively. It has been shown earlier[1,10,12] that in

phase-matching experiments, where $N_B$ is normally much larger than $N_A$ and the buffer gas has no resonances near $3\omega$, the phase mismatch $\Delta k$ can be conveniently broken up into nonresonant and resonant parts. The nonresonant part $\Delta k_0$ is almost frequency independent, and with $N_B \gg N_A$ it is proportional to $N_B$. The resonant contribution, $\kappa/\Delta_r$, can be quite large and strongly frequency dependent. It is proportional to $N_A$ and inversely proportional to the detuning from exact resonance. We have previously defined[1] the detuning from exact resonance as $\Delta_r = 3\omega - \omega_r$, where $\omega$ is the laser frequency and $\omega_r$ is the resonant line frequency. We can then write the mismatch as[1] $\Delta k = \Delta k_0 + \kappa/\Delta_r$, where $\kappa = 2\pi\omega_r N_A |D_{1,0}|^2/\hbar c$. In a negatively dispersive region the resonant contribution to the phase mismatch, $\kappa/\Delta_r$, has a sign opposite to the nonresonant part, $\Delta k_0$, which is almost entirely due to a buffer gas. The $\Delta k_0$ contribution is thus proportional to $P_B$, the buffer-gas pressure, and the resonant portion is proportional to $P_A$, the pressure of the active gas. For phase matching, $\Delta k = 0$ or $\Delta k_0 = -\kappa/\Delta_r$. We designate the detuning at phase matching as $\Delta_r \equiv \Delta_m$. Thus, phase matching will occur at a detuning $\Delta_m$, where

$$\Delta_m = -\frac{\kappa}{\Delta k_0} \simeq \frac{\omega_r N_A |D_{0,1}|^2}{(3\omega/c)N_B[\chi_B(\omega) - \chi_B(3\omega)]} . \quad (10)$$

Since the above expression contains $|D_{0,1}|^2$ we can write it in terms of the oscillator strength $F_{01}$. Thus $\kappa = \pi N_A (e^2/mc) F_{01}$ and

$$\Delta_m = \frac{e^2 F_{01}}{(6m\omega/c)[\chi_B(\omega) - \chi_B(3\omega)]} \frac{N_A}{N_B} = \frac{2\pi e^2 F_{01} N_A}{n_B(\omega) - n_B(3\omega)} . \quad (11)$$

This can be written in terms of the wavelength shift $\Delta\lambda_m$ of phase matching from resonance as

$$\Delta\lambda_m = CP_A/P_B . \quad (12)$$

The phase-matching frequency can be varied over the negatively dispersive region of a given transition by adjusting the ratio of $P_A$ to $P_B$ and the phase-matching factor $C$ of Eq. (12) can be determined experimentally. (The value of $C$ is not strictly constant, but is a slowly varying function of $\lambda$.)

Thus, on the basis of our analysis, if one scans unfocused (and counterpropagating) laser beams through a mixture of active and buffer gases in the region of a three-photon resonance, where the resonance is also coupled to the ground state through a one-photon process, then a strongly enhanced signal will be observed at the resonance position and *another* enhanced signal will be observed in a narrow-frequency region on the negatively dispersive side of the resonance, where phase matching occurs. This ionization signal will be proportional to the volume integral of the third-harmonic flux, integrated over the region from which ionization is observed.[1]

In Fig. 6 we show a series of ionization signals (number of electrons liberated within the counting volume) for 1.1 Torr of xenon buffered with various partial pressures of argon. On the far right of the figure is the ionization signal at the $6s$ resonance line, produced with counterpropagating beams. The other individual peaks occur at the phase-matching frequency for the partial pressures indicated in the figure. These signals can be produced by a single-pass unfocused beam or with reflected beams, though at the phase-matching frequency the only effect of our use of a counterpropagating beam is to increase the ionization signal through the additional light intensity. With our unfocused beams the signals occur at the third-harmonic phase-matching point for each ratio of $P_A/P_B$ as indicated in Eq. (12).

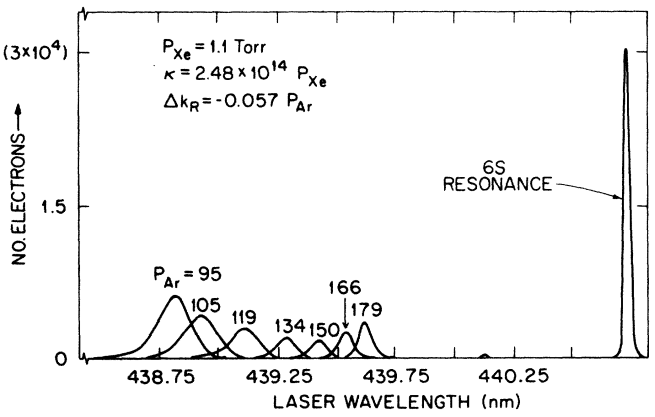


FIG. 6. Spectrum of phase-matched third-harmonic profiles in xenon with different pressures of argon buffer gas. Xenon pressure, as well as laser power, was kept constant. As the buffer-gas pressure was increased the phase-matching region moved closer to resonance. Proportional-counter gain was also kept constant. Note the small dimple at the $4f$ level; this remained constant for all the argon pressures shown. Signal at far right in the $6s$ resonance line, observable only in counterpropagating geometry.

The spectral "widths" of ionization signals produced through third-harmonic production are dependent on the number density of the buffer gas, the magnitudes of displacements from resonance $\Delta_m$, and on the absorption coefficient for the third-harmonic photons. The important effect of dimer absorption on phase-matched third-harmonic production has been included in the theoretical formalism of Ref. 1 through introduction of a small complex component $-i\beta$ in the wave-vector mismatch between fields at $\omega$ and $3\omega$, where $2\beta$ is the absorption coefficient defined above, for photons at $3\omega$. That is, the phase mismatch was generalized in the form $\Delta k = \Delta k_0 + \kappa/\Delta_r - i\beta$. The effect on third-harmonic generation of absorption in the medium was analytically described for all degrees of absorption. Detailed behavior of widths and magnitudes of MPI signals arising from the third-harmonic field will be addressed below. First, we examine measured and predicted magnitudes of third-harmonic and resonant signals as functions of gas pressure.

As was indicated in the preceding section, the analysis of Ref. 1 successfully predicts the rate of excited-state production at exact three-photon resonance for counterpropagating geometry with a fraction $f$ of the original

beam reflected back on itself. It also predicts the ionization rate which results from excitation through third-harmonic production and subsequent absorption under phase-matched conditions. For MPI at three-photon resonances and at phase-matching frequencies on the high-energy side of resonances, we can describe observed ionization signals as a product of resultant excited-state populations and an ionization rate $\gamma_I$ of the excited-state atoms. Though the ionization rate out of the excited atomic state is not independent of laser frequency, it will change little over the phase-matching frequency region of interest in the present content. If we designate the ionization rate out of the excited state at the phase-matched wavelength, which is at a detuning $\Delta\lambda_m$ from exact resonance, as $\gamma_I(\Delta\lambda_m)$, and the corresponding rate at exact three-photon resonance at $\gamma_I(0)$ (these are unmeasured in the present experiments), then the predicted *ratio* of the peaks of phase-matched to on-resonance ionization signals becomes[1]

$$\mathscr{R}_{\text{peaks}}=\frac{4\sqrt{3/2}}{9\pi}\beta\left[\frac{\Delta_m^4}{\kappa^2 L\sigma^2}\right]\frac{\gamma_I(\Delta\lambda_m)}{\Gamma_1\gamma_I(0)}\left[\frac{1+f^2}{f+f^2}\right]$$
$$\times[G_0(\xi_2,\Gamma_1,\delta_1)-G_0(\xi_1,\Gamma_1,\delta_1)]\ . \quad (13)$$

Here the magnitude of the absorption coefficient $2\beta$ is almost entirely due to mixed dimers and is proportional to the product of active-gas and buffer-gas number densities. The factor $f$ is the fraction of the laser beam which is retroreflected and overlapped with the incident beam.[1] The ratio $\gamma_I(\Delta\lambda_m)/\gamma_I(0)\sim 1$ over the range of $\Delta\lambda_m$ of interest (in the context of cross sections for ionization out of the excited state, $\Delta\lambda_m$ is very little different from zero). The analytic function $G_0(\xi,\Gamma_1,\sigma_1)$ is given by[1]

$$G_0(\xi,\Gamma_1,\delta_1)=\int_0^{\xi}d\eta\, e^{-\eta^2}\cos(\delta_1\eta)\times\left[(\xi-\eta)e^{-\Gamma_1\eta}-\frac{1}{2\Gamma_1}(e^{-\Gamma_1\eta}-e^{\Gamma_1(2\xi-\eta)})\right]. \quad (14)$$

The reduced variables are defined as $\delta_1=\sqrt{2/3}\delta/\sigma$, where $\delta$ is the detuning from exact phase matching and $\sigma$ is the bandwidth of a Gaussian laser pulse,[1]

$$\Gamma_1=\sqrt{2/3}(\gamma_{01}/2+\Delta_m^2\beta/\kappa)/\sigma$$
$$=\sqrt{2/3}[\gamma_{01}/2+\kappa\beta/(\Delta k_0)^2]$$

is an effective width for the line shape of the phase-matched signal, and $\xi=\sqrt{3/2}\sigma\kappa z/\Delta_m^2$ is a scaled $z$ coordinate along the path of the laser beam inside the medium. Thus the ratio of on-resonance and phase-matched signals can be measured and predicted to test the reliability of the theoretical analysis given previously. In Fig. 7 we show the measured and predicted pressure-dependent ratios of ionization signals at three-photon resonance to those at the phase-matched frequency for a particular

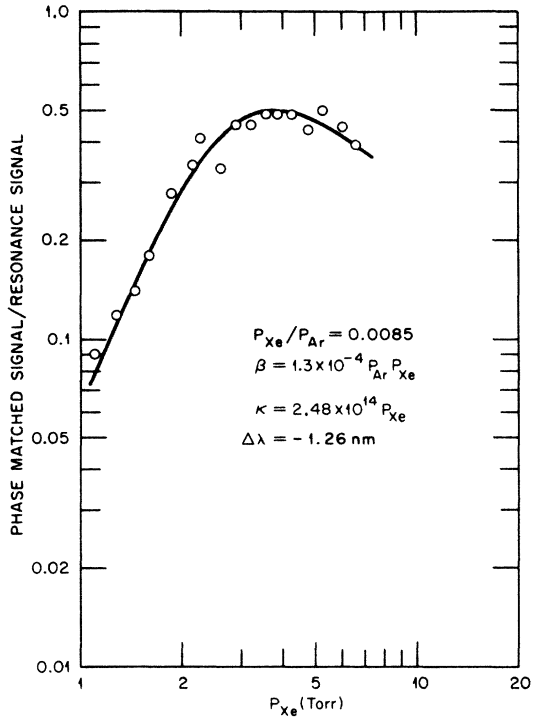


FIG. 7. Experimental and theoretical (solid line) ratios of the magnitude of the ionization signal at the phase-matched wavelength ($\Delta\lambda=-1.2$ nm for the $6s$ resonance) to the magnitude of the ionization signal at the $6s$ resonance position, as a function of $P_{Xe}$. The ratio of $P_{Xe}/P_{Ar}$ is held fixed and thus $\Delta_m$ is fixed.

$P_A$-to-$P_B$ ratio of xenon and argon. Here, the ionization cell was filled with 6.8 Torr of xenon to which 800 Torr of argon was added. This combination produced phase matching at $\Delta\lambda=-1.26$ nm from the $6s[\frac{3}{2}]$ $J=1$ three-photon resonance at 440.88 nm; that is, the sharply peaked phase-matched ionization signal occurred at 439.62 nm. After recording the data a the first point on the right of Fig. 4 (6.8 Torr xenon), the gas mixture was pumped down to successively lower pressures, where measurements were repeated to yield the series of data points in the figure. Note that the ratio $P_{Xe}/P_{Ar}=0.0085$ remained constant in this procedure and indeed the phase-matching frequency remained fixed within the bandwidth of the laser (the data were taken with the Lambda Physik apparatus with a laser bandwidth of 0.013 nm). With this procedure the third-harmonic generation and absorption as a function of total target-gas pressure was profiled for comparison with theoretically predicted behavior. In Fig. 7 we also show results from theory as the solid line. In the calculation, the laser bandwidth $\sigma=0.3\times10^{10}\ \text{s}^{-1}$, the oscillator strength was[18] $F_{01}=0.28$, $\beta=1.3\times10^{-4}P_{Xe}P_{Ar}$, and $\Delta_m$ corresponds to $\Delta\lambda_m=-1.26$ nm. The theoretical prediction of pressure-dependent third-harmonic generation and resultant MPI at a fixed phase-matching frequency agrees well with the experimental finding (also see Ref. 8). More will be said below about the shape of the curve in Fig. 7.

### D. Pressure and frequency dependences of multiphoton-ionization profiles near phase-matching frequencies

It is well known[1] that for third-harmonic generation with unfocused laser beams, if phase matching is maintained (i.e., if $\Delta k$ is kept equal to zero) while a target-gas density $N_A$ is increased, then third-harmonic production initially indicates with $N_A^2$ while the *width* of the phase-matched region decreases $\propto 1/N_A$. This behavior holds only when absorption of third-harmonic photons can be neglected. A simple illustration of the source of the narrowing of the phase-matching region with increasing pressure can be offered by noting the following: Under arbitrary conditions, when an unfocused laser beam traverses a distance from $z_1$ to $z_2$ through a nonlinear medium in which a third-harmonic field is generated, a phase difference will be accumulated between the laser field and the generated third-harmonic field which we designate as $\Delta\theta$. The total phase difference would be given by $\Delta\theta=(z_2-z_1)\Delta k$. At exact phase matching, $\Delta k=0$ and thus $\Delta\theta=0$. The "width" of the phase-matched third-harmonic profile is determined by the behavior of $\Delta\theta$ about the phase-matching point. The frequency at which $\Delta k=0$ occurs at a detuning, $\Delta_r$ (on the high-frequency side), from three-photon resonance which we defined as $\Delta_m$ (i.e., $\Delta_m$ is the value of $\Delta_r$ which produces $\Delta k=0$). Also, we have written $\Delta k=\Delta k_0+\kappa/\Delta_r$. Thus, at phase matching, $\Delta k_0=-\kappa/\Delta_m$. The behavior of phase mismatch at detunings near $\Delta_r=\Delta_m$ can be seen readily if we define $\Delta_r=\Delta_m+\delta$ (i.e., $\delta$ as defined is the distance from exact phase matching). Then,

$$\begin{aligned}\Delta\theta&=(z_2-z_1)\Delta k\\&=L\left[\Delta k_0+\frac{\kappa}{\Delta_m+\delta}\right]\\&\simeq L\left[\Delta k_0+\frac{\kappa}{\Delta_m}-\frac{\kappa\delta}{\Delta_m^2}\right],\end{aligned}\tag{15}$$

where $L=z_2-z_1$. Since $\kappa/\Delta_m$ and $\Delta k_0$ cancel, we obtain

$$\Delta\theta=\kappa L\delta/\Delta_m^2 .\tag{16}$$

An estimate of the frequency region about $\Delta_m$ where constructive interference occurs can be obtained by noting that when the phase difference $\Delta\theta$ becomes as large as $\pi$ the interference between fields generated at $z_1$ and $z_2$ becomes destructive rather than constructive. Thus the full width at half maximum (FWHM) for phase-matched third-harmonic output in a generation region of length $L$ is approximately twice the value of $\delta$ which produces $\Delta\theta=\pi$ in (16):

$$\delta_{\rm FWHM}\simeq\frac{2\pi\Delta_m^2}{\kappa L}=\frac{2\pi\Delta_m^2}{L\pi e^2F_{01}N_A} .\tag{17}$$

Note that this simple argument leads to a width which is inversely proportional to $N_A$. A more quantitative treatment[1] replaces $2\pi$ by a value of 5.56.

The particular circumstance just described was treated explicitly in Ref. 1 as case (1) (i.e., $\beta L\ll 1$ and $\sqrt{3/2}\sigma\kappa L/\Delta_m^2\ll 1$, where $\sigma$ is the laser bandwidth). The detailed theory[1] predicts that at low $N_A$, low absorption, and for $\Delta_m$ several linewidths from exact resonance, the third-harmonic signal will be generated over a frequency region of half-width

$$\delta_{\rm FWHM}=\frac{5.56\Delta_m^2}{\kappa L}=\frac{5.56mc\Delta_m^2}{L\pi e^2F_{01}N_A} .\tag{18}$$

For this case of negligible absorption the line shape for the third-harmonic flux at position $z$ along the unfocused laser beam is of the form

$$F_{3\omega}(z,t)=\frac{3|z^2N_A\kappa}{\Delta_m^2}|\alpha(\omega)|^2|\langle E_0^2(t-z/v)\rangle|^3\times\left[\frac{\sin(\kappa z\delta/2\Delta_m^2)}{\kappa z\delta/2\Delta_m^2}\right]^2,\tag{19}$$

where[1]

$$\alpha(\omega)=\sum_m D_{0,n}D_{n,m}D_{m,1}/[2\hbar^3(\omega_n-\omega_0-\omega)\times(\omega_m-\omega_0-2\omega)] ,$$

and $\langle E_0^2(t-z,v)\rangle$ designates a statistically averaged laser field.[1] We also define a three-photon Rabi frequency at the mean power density, represented through the statistically averaged field in Eq. (19), as

$$\bar{\Omega}_3(t_r)=\alpha(\omega)|\langle E_0^2(t-z/v)\rangle|^{3/2} .$$

If $N_A/N_B$ is held constant, which means that the phase-matching frequency $\Delta_m$ remains fixed, and if $N_A$ is increased, the third-harmonic flux will increase as $N_A^2$. The rate of ionization is proportional to the product of the absorption coefficient $2\beta$, multiplied by the volume integral of $F_{3\omega}$ over the portion of the laser beam that lies within the counting volume of the ionization detector and by the ionization rate out of the excited state (the rate $\gamma_I$ is not measured in these experiments; thus the absolute ionization signal must be scaled to experimental results at a single point).

The ionization rate $R_I$ for a laser of beam radius $d$, at detuning $\delta$ from exact phase matching, is[1]

$$\begin{aligned}R_I(\delta,t)&=\gamma_I 2\beta\int_{z_1}^{z_1+L}dz\int_0^\infty d\rho\,2\pi\rho e^{-6\rho^2/d^2}F_{3\omega}(z,t)\\&=\gamma_I\frac{4\sqrt{2}\pi N_A\beta}{3\sqrt{3}}d^2\left[\frac{\Delta_m^4}{\sigma^3}\right]\frac{|\bar{\Omega}_3(t)|^2}{\Gamma_1\kappa^2}[G_0(\xi_2,\Gamma_1,\sigma_1)-G_0(\xi_1,\Gamma_1,\delta_1)] ,\end{aligned}\tag{20}$$

where $G_0(\xi,\Gamma_1,\delta_1)$ was defined, by Eq. (14), with $\xi_2=\sqrt{3/2}\sigma\kappa(z_1+L)/\Delta_m^2$ and $\xi_1=\sqrt{3/2}\sigma\kappa z_1/(\Delta_m^2)$. Here the ionization volume extends from a point $z_1$ to a point $z_2=z_1+L$. [If a fraction $f$ of the beam is reflected back through the ion-

ization cell, a factor $(1+f^2)$ is required in Eq. (20)].

If phase matching occurs at detuning $\Delta_m$ from the resonance under consideration, then the frequency profile (line shape) for ionization in the low absorption limit ($\beta L \ll 1$; $\xi_1, \xi_2 \ll 1$) becomes

$$R_I(\delta,t)=\gamma_I 8\pi N_A \beta d^2 \frac{\Delta_m^4}{\sigma^2} \frac{|\bar{\Omega}_3(t)|^2}{\kappa^2\delta} \left[ \frac{\kappa\delta}{\Delta_m^2}(z_2-z_1)-[\sin(\kappa z_2\delta/\Delta_m^2)-\sin(\kappa z_1\delta/\Delta_m^2)] \right] . \quad (21)$$

In the present instance we are considering predicted behavior of MPI with a fixed $N_A/N_B$ ratio (fixed value of $\Delta_m$). Here, since $\beta \propto N_A N_B$ and $N_B \propto N_A$, then $\beta \propto N_A^2$ and the peak of the ionization signal increases as $N_A^4$. The width of the ionization profile about the phase-matching point is given by $\delta_{\mathrm{FWHM}} \simeq 7.3\Delta_m^2/\kappa L$. Thus in the low-pressure region $\delta_{\mathrm{FWHM}} \simeq 1/N_A$. If $N_A$ is increased from a very low value, then with broad-bandwidth lasers, one eventually reaches the point where $\delta_{\mathrm{FWHM}}$ becomes narrower than the bandwidth of the laser. In this limit, if $N_A$ is further increased, only a fraction of the laser light can lead to constructive interference and the generated third-harmonic light is no longer limited by the laser bandwidth. In this region the phase-matched third-harmonic flux, at fixed $N_A/N_B$ ratio, increases only linearly with $N_A$ (or ionization signals increase as $N_A^3$). Note from Eq. (18) that measurements of $\delta_{\mathrm{FWHM}}$, $\Delta_m$, and $N_A$ (the pressure of the active gas) in this region, where the ionization signal is proportional to $P_A^4$, yields the value of the oscillator strength $F_{01}$ of the electric dipole transition with which the third-harmonic generation is associated.

In Fig. 8 we show the wavelength profile or "line shape" for the ionization signal at a phase-matching wavelength corresponding to $\Delta\lambda_m = -1.004$ nm from the $5d[\frac{3}{2}]_1$ state of xenon, at a xenon pressure of 2.64 Torr (133 Torr of argon). The solid line is the theoretically predicted line shape with $\delta_{\mathrm{FWHM}}=0.0225$ nm. The actual line shape closely adheres to the predicted form given by Eq. (21).

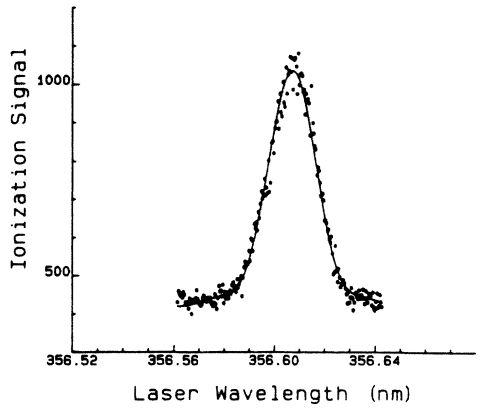


FIG. 8. Profile of a low-pressure phase-matched ionization signal near the $5d[\frac{3}{2}]_1$ level in xenon with argon buffer gas. The ratio $P_{\mathrm{Xe}}/P_{\mathrm{AR}}=0.0198$. Exact phase matching occurs at $\Delta\lambda_m = -1.004$ nm. $P_{\mathrm{Xe}}=2.64$ Torr. Solid curve is the theoretical ionization profile from Eq. (21).

We can now make some useful observations concerning the functional dependence of the data shown in Fig. 7. We noted above that at low pressure the peak of the phase-matched ionization signal should increase with the fourth power of the pressure of the active gas ($N_A^4$). The ionization signal at exact resonance should be proportional to $N_A$. Thus the ratio shown in the figure should increase as $N_A^3$ at low pressure. At pressures where the phase-matching width $\delta_{\mathrm{FWHM}}$ becomes smaller than the laser bandwidth, the form of the data in Fig. 7 should change to $N_A^2$ dependence until absorption effects begin to play a role (see below). As can be seen in the figure, and in Ref. 8, the behavior follows very closely that predicted from theory.

In Fig. 9 we show plots of measured and predicted values for the width $\delta_{\mathrm{FWHM}}$ of the ionization signal associated with phase-matched third-harmonic fields as a function of xenon pressure with krypton buffer gas at a fixed phase-matched frequency ($\Delta\lambda_m = 1.64$ nm from the $6s[\frac{3}{2}]_1$ level in xenon). The magnitude of $\delta_{\mathrm{FWHM}}$ decreases as $1/N_A$ at low pressure until it becomes limited by the laser bandwidth or by absorption processes. Again, very good agreement exists between experiment and theory. Note, in particular, that the $N_A^4$ dependence of the low-pressure ionization signal (or $N_A^3$ for the ratio in Fig. 7) confirms the dimer-absorption process described earlier.

In the above discussion of the low-pressure regime, ab-

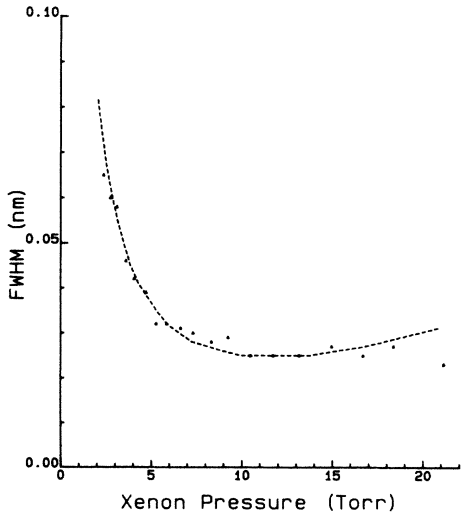


FIG. 9. Variation with xenon pressure of the full width at half maximum (FWHM) of the ionization signal at the phase-matched frequency. In this instant, phase matching occurs at $\Delta\lambda = -1.64$ nm from the $6s$ resonance in xenon with krypton buffer gas.

sorption of the generated photons could be neglected. However, it usually is the case that by the time $N_A$ is increased to the region where $\delta_{\text{FWHM}}$ becomes comparable to the laser bandwidth, linear absorption of the vuv photons from mixed dimers becomes significant. Thus absorption at $3\omega$ must be included[1] in treating third-harmonic generation. This has been done in I through inclusion of an absorption coefficient $2\beta$ in the formalism ($\beta \propto P_A P_B$). Once the absorption length of the generated photons become smaller than $L$, the length of the nonlinear medium, then constructive interference occurs between fewer active atoms along the laser beam. This feature of third-harmonic generation has been treated in detail in I, where it was shown that $\delta_{\text{FWHM}}$ for third-harmonic generation is strongly influenced by the absorption. Indeed, once $1/2\beta < L$ the constructive interference between third-harmonic field contributions from subsequent "downstream" atoms is limited to a distance $\sim(1/2\beta)$. Thus, $L$ in Eq. (1) is replaced by a quantity proportional to $1/\beta$. In this high-pressure, high-absorption limiting case [case (3) of I] the phase-matching region is characterized by a phase-matching frequency profile with a width which is proportional to the absorption coefficient. That is,[1]

$$\delta_{\text{FWHM}} = 2\beta\Delta_m^2/\kappa \ . \tag{22}$$

However, as mentioned above if $P_A/P_B$ is held fixed (phase matching occurring at fixed displacement $\Delta_m$), then $P_B \propto P_A$ and $\beta \propto P_A^2$. Thus, in the high-pressure limit where $\beta L \gg 1$, we have $\delta_{\text{FWHM}} \propto P_A \Delta_m^2$. In the data shown in Fig. 9 the highest pressures studied were just at the regime where the width becomes linear with $P_{\text{Xe}}$. A better example, which is in very good agreement with this prediction, is given in Fig. 6 of Ref. 8.

Under the present circumstances, where absorption is large, the rate of ion production integrated over the laser volume is given by

$$R_I(\delta_I,t) = \gamma_I \frac{2\pi N_A d^2 \Delta_m^2 \beta}{\kappa\sigma^2} |\Omega_3(t)|^2 \times \frac{1}{\delta^2 + \Delta_m^4 \beta/\kappa^2}(z_2 - z_1) \ . \tag{23}$$

In this pressure region the third-harmonic flux is proportion to $N_A^{-2}$. The peak of the ionization signal at a fixed phase-matched frequency becomes independent of $N_A$, or as shown in Fig. 7, the ratio of the phase-matched to the resonance ionization signals becomes proportional to $N_A^{-1}$ as predicted.

We further note that the predicted frequency profile for phase-matched third-harmonic generation in the high-absorption region is Lorentzian.[1] In Fig. 10 we show experimental and theoretical line shapes for the phase-matched ionization signal near the $5d[\frac{3}{2}]_1$ level of xenon. In the example shown, $P_{\text{Xe}} = 4.04$ Torr, $P_{\text{Ar}} = 701$ Torr, and phase matching occurs at $\Delta\lambda_m = -2.47$ nm. The FWHM of the case shown in the figure was $\delta_{\text{FWHM}} = 0.0079$ nm.

All of the experimental results at high pressures conform well with the predictions of paper I. Note that in a given set of measurements of the MPI signals at different

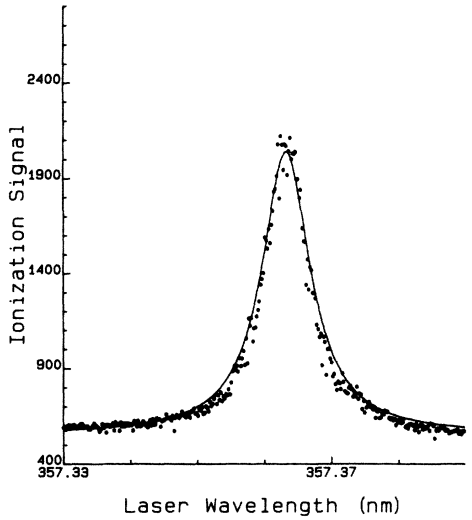


FIG. 10. Profile of a high-pressure MPI signal in the region of phase matching in xenon with argon buffer gas. In these data $\Delta\lambda_m = -0.247$ nm for $P_{\text{Xe}} = 4.04$ Torr and $P_{\text{Ar}} = 701$ Torr. The solid line is a theoretically predicted ionization line shape for this circumstance.

pressure under fixed $P_A/P_B$, the low-pressure behavior can be used to determine $F_{01}$, or $\kappa$, through Eq. (18). Then from measurements in the same mixture at high pressure, Eq. (22) can be used to determine $\beta$, the absorption coefficient.

The results presented so far in this section have demonstrated good agreement between theory and experiment in two limiting cases and they have illustrated how an oscillator strength $F_{01}$ and an absorption coefficient $\beta$ can be obtained from the measurements. Indeed, if we refer back to Eq. (3) we see that having determined $F_{01}$, or $\kappa$, we can use a measurement of

$$\Delta_m = -\kappa/\{3\omega/c[n_B(\omega) - n_B(3\omega)]\}$$

to determine the difference in the index of refraction of the buffer gas at $\omega$ and $3\omega$. Since the index in the visible or near-visible region, $n_B(\omega)$, is usually known accurately, one can thus determine $n_B(3\omega)$, the index at the third-harmonic frequency where it is often not accurately known. (In the vuv in the present context.)

We hasten to add that the above limiting cases were chosen only for illustrative purposes. Theoretical analysis of Ref. 1 provides a quantitative description of the MPI processes over wide spectral and pressure ranges with good agreement with experiment at all pressures and under all phase-matching frequencies over the negatively dispersive regions of several xenon levels. Moreover, as stated previously,[8] the detailed description of ionization processes in the phase-matching region allows an accurate determination of $F_{01}$, $\beta$, and $n_B(3\omega)$, not through use of the simple limiting cases represented in Eqs. (17) and (22) above, but through a detailed match of theory with experiment as represented, e.g., in Fig. 9. By adjusting values of the oscillator-strength absorption coefficient and refractive index in a computer-generated match to experi-

mental data at a particular phase-matching frequency, one can simultaneously determine all three of these optical constants from one set of experimental data. The analysis can be carried out for any particular ratio of $P_A/P_B$; that is, at any choice of phase-matching frequency. The theoretical analysis applied in Fig. 9 produced values of 0.26 for the oscillator strength, $F_{01}$, of the $6s\,(J=1)$ level in xenon and an absorption coefficient $2\beta=1\times10^{-4}P_{\mathrm{Xe}}P_{\mathrm{Kr}}$ ($\mathrm{cm}^{-1}$) with $P$ in Torr. Also, we obtained for krypton an index of refraction per atom of $[n_{\mathrm{Kr}}(3\omega)-1]/N_{\mathrm{Kr}}=2.61\times10^{-23}$ $\mathrm{cm}^{-3}$ at $\lambda_{3\omega}=146.4$ nm. A more complete study of determinations of vuv optical constants by the present method including comparisons with results from other methods will be published separately.[19]

### E. Effect of third-harmonic absorption on ionization through a $4f\,(J=2)$ level in xenon

With reference to Fig. 6, we have noted that the off-resonance ionization processes are dominated by third-harmonic absorption and that the phase-matched third-harmonic wavelength, i.e., the value of $\lambda$ at which third-harmonic photons are produced, can be "scanned" by varying $P_{\mathrm{XE}}/P_B$. This property can be used to explore the effect of third-harmonic light on a transition which can be induced by four laser photons or by one third-harmonic photon plus one laser photon, such as the $4f[\frac{3}{2}]$ $J=2$ level, which is in the negatively dispersive region of the $6s$ state of xenon. Note in Fig. 6 that a very small enhancement in the ionization signal exists at the wavelength for four-photon excitation of the strongest of the $4f$ transitions. Under the conditions illustrated in the figure, there are no third-harmonic photons at the resonance wavelength for four-photon excitation of the $4f$ level. In this instance we call attention to the fact that the resonant $4f[\frac{3}{2}]$ $J=2$ signal is quite small as compared to either the phase-matched or three-photon resonance (counterpropagating) signals. This behavior contrasts sharply with previously reported MPI spectra of xenon in which *focused* beams were utilized.[2,4,14] In these earlier studies, $4f$ ionization signals were very prominent features of the xenon spectra. However, we note that in a focused geometry, third-harmonic photons are produced on the blue side of the $6s[\frac{3}{2}]$ $J=1$ resonance, and this third-harmonic generation produces very effective pumping of two of the $4f$ levels by *two* photons (one third-harmonic plus one laser photon) as opposed to the normal four-photon excitation of these levels. This can be usefully and quantitatively illustrated as follows.

Consider excitation of a two-photon resonance by photons of frequencies $\omega_1$ and $\omega_2$, where $\hbar(\omega_1+\omega_2)$ corresponds to the energy of the allowed two-photon resonance. The two-photon state is pumped at a rate

$$R\simeq|\Omega_2|^2/\Gamma_L\ , \tag{24}$$

where $\Omega_2$ is the two-photon Rabi frequency evaluated at the average power density and $\Gamma_L$ in the larger of the two bandwidths of the photon sources. This approximate equation is based on the assumption that $|\Omega_2|\ll\Gamma_L$, and the separation between modes in the laser beams is smaller than the Doppler width, which, in turn, is smaller than $\Gamma_L$. With an added condition, namely the presence of a near-resonant one-photon intermediate resonance (which is appropriate to our present considerations), the sum over intermediate state which determine $\Omega_2$ can be approximated by the dominant term as

$$|\Omega_2|\simeq|\Omega_{01}|\ |\Omega_{12}|/\Delta\ , \tag{25}$$

where $|\Omega_{01}|$ is a one-photon Rabi frequency between the ground state and the dominant intermediate state, $|\Omega_{12}|$ is the one-photon Rabi frequency between the intermediate state and the upper two-photon state, and $\Delta$ is the detuning in frequency units from the intermediate resonance. In our cases, we typically would have $|\Omega_{01}|\simeq10^8\sqrt{I_2}$, $|\Omega_{12}|\simeq10^8\sqrt{I_1}$, and $\Delta\simeq1.5\times10^{15}\epsilon$, where $\epsilon$ is the detuning in eV and $I_1$ and $I_2$ are intensities in $\mathrm{W/cm}^2$. Thus as an order of magnitude, we have

$$|\Omega_2|\simeq6(I_1I_2)^{1/2}/\epsilon\ .$$

For $\Gamma_L\sim1\ \mathrm{cm}^{-1}$ we have the excitation rate, Eq. (23), in the form

$$R\simeq2\times10^{-10}I_1I_2/\epsilon^2\ . \tag{26}$$

Now suppose that $\omega_1$ is a laser frequency and $\omega_2$ is the third-harmonic field. We can also write the rate $R$ in terms of a flux of third-harmonic photons (i.e., $\omega_2$) and an effective cross section for their absorption. In our xenon example we have

$$R=\sigma_2\Phi_2\simeq\sigma_2I_2/1.6\times10^{-18}\ \mathrm{J/photon}\ ,$$

or

$$\sigma_2\simeq3\times10^{-28}I_1/\epsilon^2\ , \tag{27}$$

where $\sigma_2$ is in $\mathrm{cm}^2$ when $I_1$ is in $\mathrm{W/cm}^2$ and $\epsilon$ is in eV. Even if $\epsilon\sim0.5$ eV from intermediate resonance, we have $\sigma_2\sim10^{-18}$ $\mathrm{cm}^2$ for a laser intensity of $10^9$ $\mathrm{W/cm}^2$. This effective cross section for absorption of the third-harmonic photon can be quite large. In our example, if the concentration of the active gas is higher than $\sim10^{18}$ $\mathrm{cm}^{-3}$, then at laser intensities greater than $10^9$ $\mathrm{W/cm}^2$ third-harmonic photons generated at the frequency of a two-photon resonance involving one third-harmonic photon and one laser photon, will be strongly absorbed. The cross section for absorption through the two-photon process is proportional to the laser intensity. Thus, upon tuning through such a resonance one would expect to see a dip in the third-harmonic photon output at the resonant frequency. This effect has been observed in third-harmonic generation in xenon.[4]

If multiphoton ionization is being observed, then a strong peak in ion current will be observed at the two-photon resonance. This corresponding effect has also been observed experimentally in the MPI studies involving excitation of $4f$ levels in xenon. However, in previous studies, the relative effectiveness of the two-photon excitation involving third-harmonic generation versus four-photon excitation is difficult to extract from earlier stud-

ies since the two processes cannot easily be separated in experiments on these particular transitions when utilizing focused beams.

As we have already seen, the use of an unfocused geometry and a positively dispersive buffer gas allows us to generate third-harmonic photons in a narrow frequency region which can be shifted at will by changing $P_{Xe}/P_B$. Thus, we can clearly illustrate the effectiveness of third-harmonic pumping of a $4f$ level by "tuning" the phase-matched third-harmonic output across the frequency position of the four-photon (or two-photon using one third-harmonic photon plus one laser photon) resonance. Experimental results from this procedure are compiled in Fig. 11. In these data, $P_{Xe}=0.76$ Torr. The ionization signal on the right of each panel of the figure is that produced by counterpropagating beams at the $6s$ resonance. The $6s$ resonance signal is independent of $P_{Ar}$. Starting on the upper-left panel of the figures, we see a series of spectra which show three peaks in the ionization signals. The peak on the far left (in the first panel) is the ionization due to phase-matched phase-harmonic production. The position of this peak is controlled by the buffer-gas pressure $P_{Ar}$. The peak at 440.3 nm which is very small in the first trace, arises from four-photon pumping of the $4f[\frac{3}{2}]$ $J=2$ level of xenon. At $P_{Ar}=114$ Torr no third-harmonic light is generated at the $4f$ resonance position and the ionization signal is indeed very small ($\sim 100$ electrons). However, the third-harmonic photon output can be moved to overlap the $4f$ resonance by varying $P_{Ar}$. Thus in the trace at the upper right, where $P_{Ar}=177.8$ Torr, the phase-matched third-harmonic peak almost overlaps the $4f$ resonance and the $4f$ peak is significantly increased by the contribution to the excitation process from the few third-harmonic photons that are present on the long-wavelength "wing" of the phase-matching third-harmonic production. But at 202.2 Torr of argon buffer gas, the phase-matching point for third-harmonic production coincides with the frequency for third-harmonic photons which can, in combination with one laser photon, resonantly pump the $4f(J=2)$ through two-photon excitation. Here the ionization signal increases dramatically to 33 500 electrons. (Only two peaks appear in this panel since the $4f$ and third-harmonic peaks coincide.) In the last panel, where $P_{Ar}=250.5$ Torr, the third-harmonic peak has moved to longer wavelengths, and the $4f$ peak is small again. Thus, even though the intensity of ultraviolet photons in these studies is only about $10^{-5}$ that of the laser, the two-photon pumping rate is enormous as compared to four-photon excitation, leading to a great enhancement of the $4f$ excitation when third-harmonic photons are present. It is quite evident that a complicated pressure dependence of the $4f$ signals seen in earlier experiments[2,4,14] is to be expected since both the third-harmonic generation and the gain of the proportional counters were affected by changes in the xenon pressure.

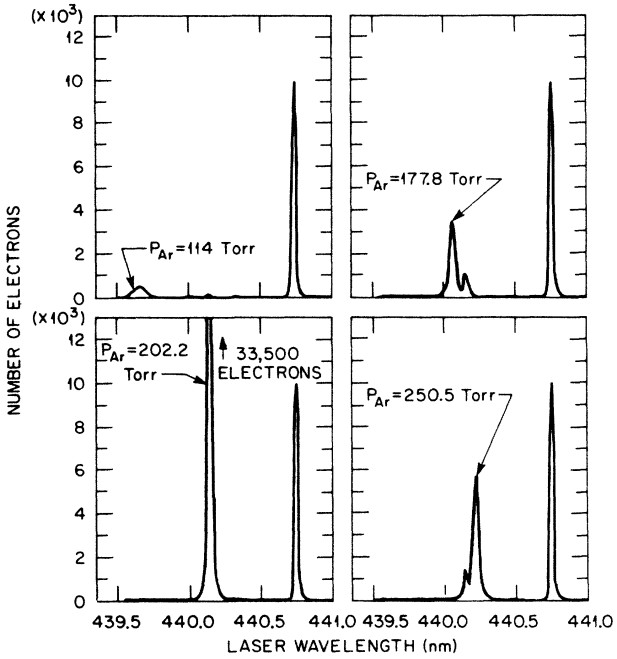


FIG. 11. Series of experiments designed to show the effect of third-harmonic pumping on a transition which can be excited by four laser photons, or one third-harmonic photon plus one laser photon. $P_{Xe}=0.76$ Torr. On the far right of each panel is the $6s$ three-photon resonance. In the procedure illustrated here the buffer-gas pressure is sequentially increased so that phase-matched third-harmonic light is "marched" across the wavelength position which is in two-photon resonance (one third-harmonic plus one laser photon) with the $4f$ level. The presence of third-harmonic photons leads to very strong enhancement in the excitation of the $4f(J=2)$ level.

## IV. CONCLUSIONS

We have tried to systematically characterize MPI processes in noble gases in the vicinity of three-photon $\Delta J=1$ resonances. The study has confirmed detailed theoretical predictions of the role of third-harmonic fields in such studies, and it has illustrated how such a detailed description of phase-matched third-harmonic generation, as measured with MPI techniques, may be used to determine vuv oscillator strengths, absorption coefficients, and vuv indices of refraction for the buffer gas, all in the same experiment and with the use of visible photons. A directed application of the MPI method to determination of vuv optical constants will be the subject of a separate study.[19] Finally, we have been able to make a quantitative illustration of the role which third-harmonic production can play in multiphoton ionization of resonances which can be excited by four laser photons or by one third-harmonic plus one laser photon.

## ACKNOWLEDGMENTS

This research was sponsored by the Office of Health and Environment Research, U.S. Department of Energy, under Contract No. DE-AC05-84OR21400 with Martin Marietta Energy Systems Inc. One of us (W.R.F.) received support from the U.S. Department of Energy through the Oak Ridge Associated Universities.

[1]M. G. Payne, W. R. Garrett, and W. R. Ferrell, preceding paper (hereafter referred to as paper I), Phys. Rev. A **34**, 1143 (1986).
[2]J. C. Miller, R. N. Compton, M. G. Payne, and W. R. Garrett, Phys. Rev. Lett. **45**, 114 (1980).
[3]R. N. Compton, J. C. Miller, A. E. Carter, and P. Kruit, Chem. Phys. Lett. **71**, 87 (1980).
[4]J. C. Miller and R. N. Compton, Phys. Rev. A **25**, 2056 (1982).
[5]J. H. Glownia and R. K. Sander, Phys. Rev. Lett. **49**, 21 (1982).
[6]D. J. Jackson and J. J. Wynne, Phys. Rev. Lett. **23**, 543 (1982).
[7]D. J. Jackson, J. J. Wynne, and P. H. Kes, PHys. Rev. A **28**, 781 (1983).
[8]M. G. Payne, W. R. Ferrell, and W. R. Garrett, Phys. Rev. A **27**, 3053 (1983).
[9]M. G. Payne, W. R. Garrett, and H. C. Baker, Chem. Phys. Lett. **75**, 468 (1980).
[10]M. G. Payne and W. R. Garrett, Phys. Rev. A **26**, 356 (1982).
[11]M. G. Payne and W. R. Garrett, Phys. Rev. A **28**, 3049 (1983).
[12]J. J. Wynne, Phys. Rev. Lett. **52**, 741 (1984).
[13]G. S. Agarwal and S. P. Tewari, Phys. Rev. A **29**, 1922 (1984).
[14]K. Aron and P. M. Johnson, J. Chem. Phys. **67**, 5099 (1977).
[15]G. S. Hurst, M. N. Nayfeh, and J. P. Young, Appl. Phys. Lett. **30**, 299 (1977).
[16]M. C. Castex, J. Chem. Phys. **66**, 3854 (1977).
[17]R. N. Compton and J. C. Miller, J. Opt. Soc. B **2**, 355 (1985).
[18]G. I. Chashchina and E. Y. Shreider, Opt. Spectrosc. **27**, 79 (1969).
[19]W. R. Ferrell, W. R. Garrett, and M. G. Payne (unpublished).

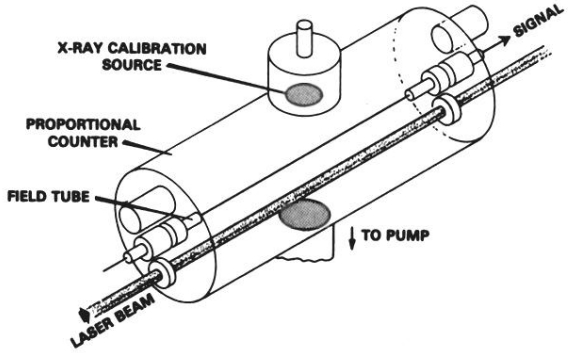


FIG. 1. Proportional counter showing field tubes or guard rings, removable x-ray calibration source, and laser-beam path. Length of proportional counter region between field tubes is 11.5 cm.